2018

Room Temperature Operation of Quantum Cascade Lasers Monolithically Integrated Onto a Lattice-Mismatched Substrate

Rowel Go
University of Central Florida

ROOM TEMPERATURE OPERATION OF QUANTUM CASCADE LASERS

MONOLITHICALLY INTEGRATED ONTO A LATTICE-MISMATCHED SUBSTRATE

by
ROWEL CANAON GO
B.S. University of California, Los Angeles 1999

A thesis submitted in partial fulfillment of the requirements
for the degree of Master of Science
in The College of Optics & Photonics
at the University of Central Florida
Orlando, Florida

Summer Term
2018

Major Professor: Arkadiy Lyakh

ABSTRACT

Quantum Cascade Lasers (QCLs) are semiconductor devices that, currently, have been observed to emit radiation from ~ 2.6 μm to 250 μm (1 to 100 terahertz range of frequencies.) They have established themselves as the laser of choice for spectroscopic gas sensing in the mid-wavelength infrared (3-8 μm) and long-wavelength infrared (8-15 μm) region. In the 4-12 μm wavelength region, the highest performing QCL devices, in terms of wall-plug efficiency and continuous wave operation, are indium phosphide (InP) based. The ultimate goal is to incorporate this InP-based QCL technology to silicon (Si) substrate since most opto-electronics are Si-based. The main building blocks required for practical QCL-on-Si integrated platforms will be covered in this work. InP is lattice-mismatched to gallium arsenide (GaAs), even though both are III-V compound semiconductor materials. The first room temperature operation of QCL grown on a lattice-mismatched GaAs substrate with metamorphic buffer (M-buffer) is discussed in this thesis. The QCL structure's strain-balanced active region was made up of 40-stages of alternating barriers ($Al_{0.78}In_{0.22}As$) and wells ($In_{0.73}Ga_{0.27}As$) and an all-InP, 8 μm-thick waveguide. A small sample of 2 cm^2 size was taken from a 6-inch wafer and processed into ridge-waveguide chips 3 mm x 30 μm in size. Lateral current injection scheme was utilized due to an insulating M-buffer layer. Preliminary reliability testing up to 200 minutes of runtime showed no sign of power degradation. Laser chips with high reflection (HR) coating showed optical power over 200 mW of total peak power at cryogenic temperature (78 K), with lasing seen up to 230 K. In this temperature range, the measured characteristic temperatures of $T_0 \approx 460$ K and $T_1 \approx 210$ K describes the temperature dependence for threshold current and slope efficiency. Adding a partial HR coating (56%) on the front facet extended the lasing range above room temperature (303 K). This thesis will also discuss

the preliminary cryogenic temperature result of the first InP-based QCL grown on lattice-mismatched silicon (Si) substrate.

This work is dedicated to anyone who cares enough to read it.

ACKNOWLEDGMENTS

This work was accomplished with the help of Professor Arkadiy Lyakh, the principal investigator of the projects that this work covers, the designer of the quantum well superlattices that are used, and a provider of guidance and advise throughout the process of this work. IQE for growing the materials. Pedro Figueiredo for the help with mask design and the test setup. Matthew Suttinger provided formatting help and guidance with the writing of this thesis.

TABLE OF CONTENTS

LIST OF FIGURES

LIST OF ACRONYMS/ABBREVIATIONS

AFM – Atomic Force Microscope

AlN – Aluminum Nitride

CoC – Chip-on-Carrier

EL – Electroluminescence

FWHM – Full Width at Half Maximum

GaAs – Gallium Arsenide

HBr – Hydrobromic Acid

HR – Highly Reflective

InP – Indium Phosphide

LASER – Light Amplification by Stimulated Emission of Radiation

L-I – Light-Current

MBE – Molecular Beam Epitaxy

MOCVD – Metal Organic Chemical Vapor Deposition

NRR – Non-Radiative Electron-Hole Recombination

PECVD – Plasma-Enhanced Chemical Vapor Deposition

QCL – Quantum Cascade Laser

RWG – Ridge Waveguide

SEM – Scanning Electron Microscope

Si – Silicon

T_0 – The Characteristic Temperature of Pulsed Slope Efficiency

T_1 – The Characteristic Temperature of Threshold Current Density

CHAPTER 1: INTRODUCTION

Ever since their first demonstration in 1994 [1], Quantum Cascade Lasers (QCLs) have slowly entrenched themselves as the standard semiconductor laser source in the mid-infrared region. This is due to the fact that, unlike diode lasers whose wavelengths are mainly determined by the material bandgap, ranging from visible to near infrared [2], the emission wavelength of QCLs can be vastly engineered from about 3-250 μm depending on the thickness of barrier and wells composing the laser core heterostructure, and the material system being used. QCL operate on the principle of quantum confinement of electron wavefunctions within the conduction band of a heterostructure. It consists of periodic series of thin layers of varying material composition forming a superlattice. The idea of achieving lasing using intersubband transitions in a repeated stack of semiconductor multiple quantum well heterostructures (superlattice) was first proposed in 1972 [3].

The broad coverage of QCL in the 3-14 μm spectral region is very important in the field of spectroscopy since many trace gases have strong fundamental rotational-vibrational transitions in this range [4]. Some QCL applications being explored are: range detection of explosive material with optical spectroscopy [5], infrared countermeasures [6], frequency comb generation [7], and medical diagnostics [8].

The complication of III/V compound semiconductor device integration onto lattice-mismatched substrates usually arises in the domain of silicon-based optoelectronics. It has always been the objective to combine the advantage of a low cost, large substrate area epi-growth inherent to the silicon technology with the high speed, imaging, and sensing capabilities of III/V light emitting devices [9]. QCLs are especially attractive for integration onto low cost substrates. The

theoretical modulation rate limit of these semiconductor devices are on the order of tens of GHz. Also, depending on the applied bias, QCL structures can be designed to operate either as a laser source or as a photodetector [10]. Because of these, they can be used for monolithic and cross talk-free optical interconnects. As mentioned above, QCLs have already established themselves as the technology-of-choice in spectroscopy since they cover the fingerprint infrared spectral region. The validation of frequency comb operation [11] for broad-gain QCLs further substantiates the possibility of ultra-compact dual comb sensors fully integrated onto a silicon substrate. Similarly, ring-cavity surface-emitting QCLs [12] can be used for standoff detection, as pixels for infrared displays, and for infrared illumination.

The primary technical hurdle with monolithic integration of III/V devices onto lattice-mismatched substrates is the formation of misfit dislocations, which in turn produce threading dislocations that propagate into the active region. These threading dislocations create non-radiative electron-hole recombination (NRR) centers in p-n junction devices, which limits device performance and reliability [13]. Since QCLs are unipolar devices, the problem of carrier leakage via mid-gap states is alleviated as their presence leads to carrier depletion in the proximity of the dislocation rather than to NRR. In this work, we discuss the experimental results of room temperature operation of QCLs monolithically integrated onto a lattice-mismatched GaAs substrate. This will ultimately springboard the development of monolithic QCL-on-Si platforms for a wide range of important applications.

Chapter 2 gives an overview on the basic principle of quantum cascade lasers. Chapter 3 discusses how InP-based QCL are generally grown. Step-by-step wafer processing and experimental results of InP-based QCLs on GaAs substrate are covered in Chapter 4. Next, we

look at the experimental results of InP-based QCLs on Si substrate in Chapter 5. Lastly, Chapter 6 provides a conclusion to the results of these efforts and the future direction of this research.

CHAPTER 2: BASICS OF QUANTUM CASCADE LASERS

Quantum Cascade Lasers operate entirely in the conduction band. This is the main difference between a QCL and a standard diode laser, which rely on the transition of electrons from the conduction band to the valence band to emit photons (see Figure 1). QCL utilizes bandgap engineering to construct a superlattice of semiconductor materials that leads to the creation of a potential well structure. Under electrical bias, this well structure is the source of the laser light. The superlattice is often referred to as the active region.

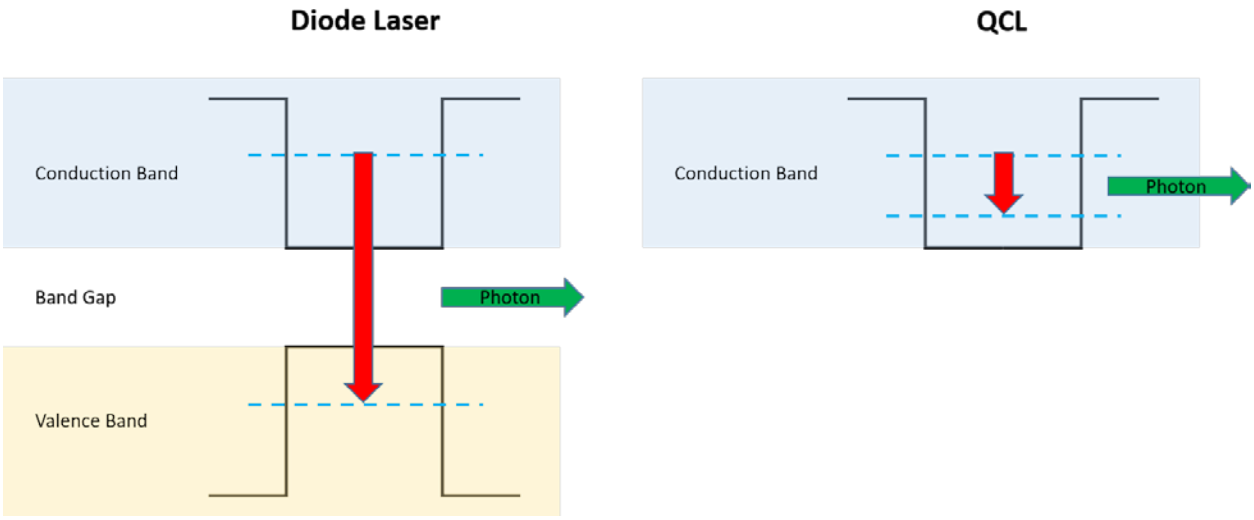

Figure 1: Comparison lasing schemes for a standard diode laser and a quantum cascade laser.

Section 1: Lasers

LASER is an acronym for light amplification by stimulated emission of radiation. Laser light is created when an incoming photon causes a transition of an electron from an upper laser energy level to a lower laser level, resulting in the stimulated emission of an identical photon with identical phase. For this to occur, the incoming photon (and thus the identical outgoing photon) must have an energy level equal to the difference of the upper and lower laser energy levels.

In a large population of electrons, the population of electrons in the upper laser level must be greater than that of the lower laser level for a net output of laser light to be statistically favorable. This is phenomenon is called population inversion. Without population inversion, an incoming photon will likely be absorbed by an electron in a lower laser level, causing a transition to an upper laser level.

Section 2: The Superlattice

The QCL superlatice is a periodic heterostructure made up of ternary semiconductor materials forming barriers and wells (see Figure 2). Lower bandgap materials (i.e., InGaAs) serve as quantum wells when adjoining to higher band gap materials (i.e. AlInAs), which serve as barriers. Each stage, or period, is comprised of an active region and an injector region. The active region's purpose is to localize the laser levels within relatively wide quantum wells. The injector region's function is to transport electrons out of lower laser level toward the next stage of the superlattice to maintain population inversion (see Figure 3). QCL devices are driven at a DC bias, giving the well structure a slope. Electrons transport from the first to last stage of the QCL structure through tunneling and scattering effects.

Transitions between states occur when the energy difference between states is bridged by the electron's absorption or emission of energy to the exact amount of energy difference. In a QCL, this can be in the form of photons (the quantum of light,) phonons (the quantum of collective vibrational excitation in a periodic structure,) or scattering.

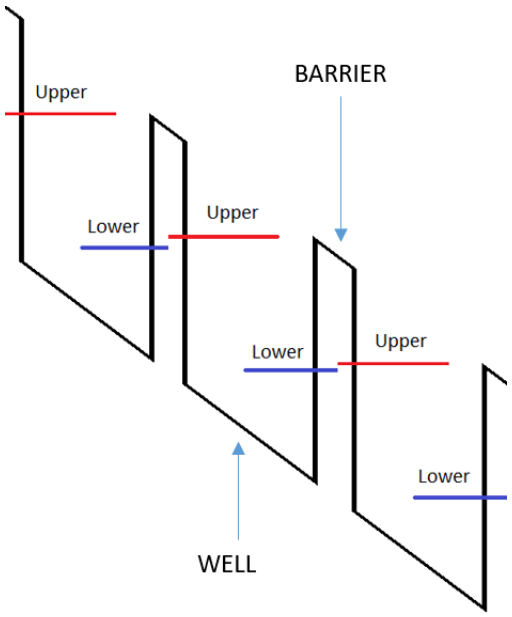

Figure 2: Simplified two level QCL showing barriers and wells that are periodically repeated. The potential, shown in black, is a series of quantum wells that are coupled by proximity. Upper and lower energy levels are shown as red and blue lines, respectively. Due to voltage bias, electrons tunnel through barriers from lower levels in one well to the upper level in the next well with lower potential energy.

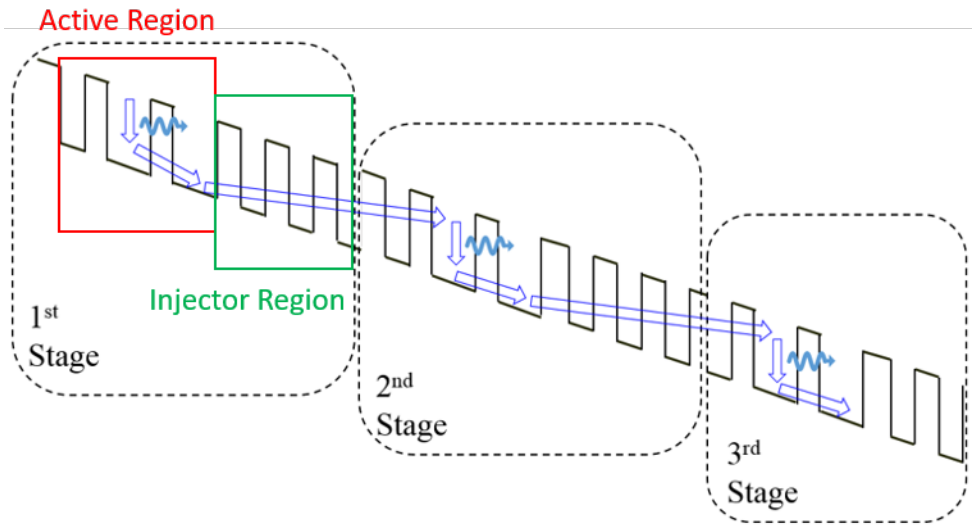

Figure 3: Illustration of the cascading structure of QCL. The active region is where the actual lasing occurs, and injector region is where the electron is transported to the next stage of the superlattice.

Section 3: Typical Active Region Design

A typical QCL structure is shown in Figure 4. The upper laser level is labeled as 4 and the lower laser level is labeled as 3. Electrons are injected into level 4, then transition to level 3 via spontaneous or stimulated emission. Level 3 is depopulated via phonon scattering. The level just below state 4 is called the injector (ground) state. Its function is to move the electrons into the next period of the superlattice. This injector state has high overlap and very close energy level correspondence with the subsequent level 4. This leads to a high injection efficiency, η_i, which is the probability that electrons from the previous injector state will be injected to the upper laser level of the next stage and then stimulated into releasing a photon.

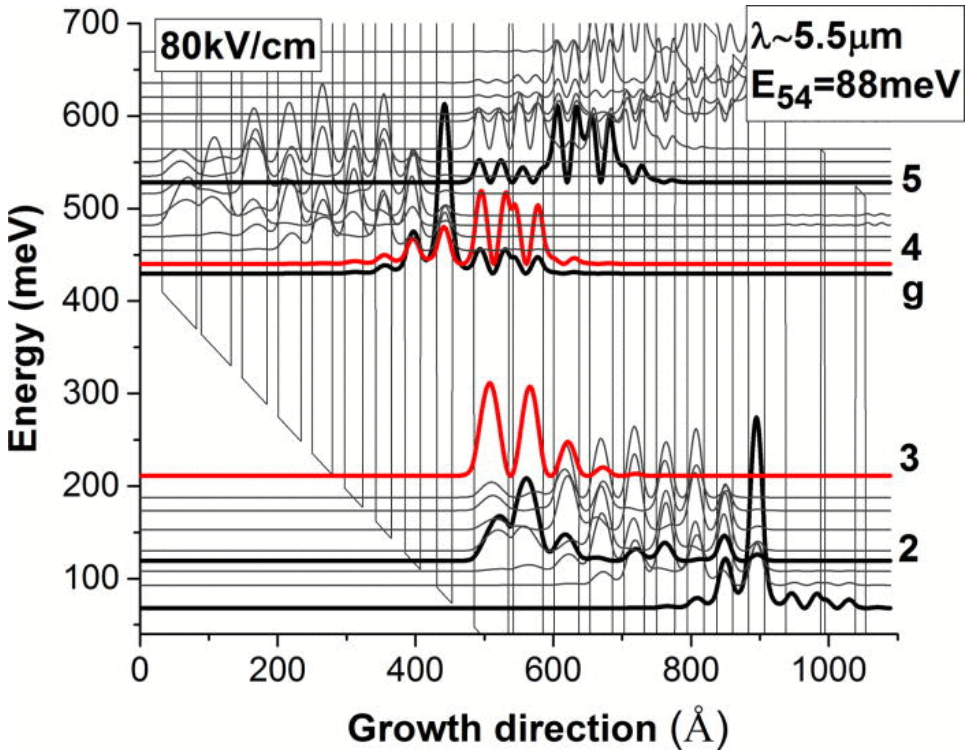

Figure 4: A typical QCL active region design. The thin black line pattern on the the background represent the potential energy profile experienced by the active region when DC bias is applied. The active region is composed of a series of barriers (AlInAs) and wells (InGaAs). The wavefunctions produced by the potential are shown as curves. Relevant states are shown as thick curves. The upper laser level 4 and lower laser level 3 are in red.

Electron injection to the subsequent stage is not certain. It can decay non-radiatively from the injector to lower levels. Electrons can also escape into continuum, or can transition to higher energy levels called parasitic states (see level 5 highlighted on Figure 4). Electrons in the parasitic state are not be able to contribute to the lasing scheme of the 4-3 transition levels. These non-radiative transitions only contribute to heat generation because conversion to photon energy does not occur.

Voltage defect is the net transition energy from the lower laser level of one stage to the upper laser level of the next stage. Again, these transitions are non-radiative, therefore energy is released in the form of heat. Voltage defect is crucial for electron transport as it prevents backscattering of the proceeding upper laser level to the previous lower laser level. Strong backscattering would occur if there were not enough injector length and energy level difference.

Section 4: Waveguides

Confining light within a small region of space is the main function of optical waveguides. Using the principle of Snell's Law, optical wave guiding is accomplished by carefully choosing materials that has higher refractive index in the region where light is to be confined, and lower refractive index around the said region. The surrounding materials are often referred to as the cladding layers. Figure 5 shows the waveguide used for the materials in this thesis.

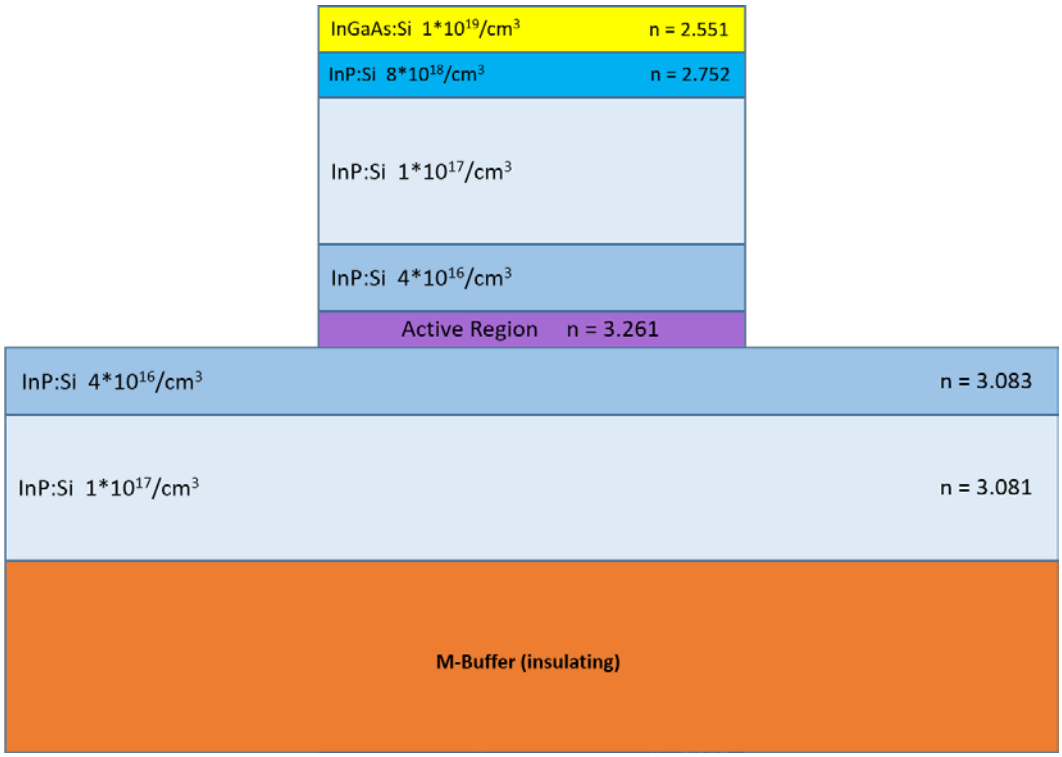

Figure 5: A schematic of the waveguide used for the devices in this work. The active region is comprised of a superlattice of indium gallium arsenide and aluminum indium arsenide. The cladding layers are composed of indium phosphide doped with silicon. The dopants purpose is to carry charge and to modify refractive index.

The refractive index, n, is a complex value. The real portion characterizes the phase velocity whereas the complex portion pertains to the losses associated with travelling through the waveguide, α_{WG}. Below is a summary of the relationship (λ_0 is the vacuum wavelength of light and β is the propagation constant):

$$n = n' + i\,n'' \tag{1}$$

$$k_0 = \frac{2\pi}{\lambda_0} \tag{2}$$

$$\beta = k_0 n' \tag{3}$$

$$\alpha_{WG} = 2k_0 n'' \tag{4}$$

Our QCLs are edge-emitting devices that have Fabry-Perot cavity configurations. In this case, the waveguide is cleaved to length L and the flat facets provide interfaces for transmission and reflection. Mirror loss is the light lost through transmission at the facets from the waveguide to some external material. It is also a function of reflection R:

$$R = \left|\frac{n - n_{external}}{n + n_{external}}\right|^2 \tag{5}$$

$$\alpha_M = \frac{-\ln(R_1 R_2)}{2L} \tag{6}$$

For the equation above, R_1 and R_2 refers to reflection at the first and second interfaces of the Fabry-Perot cavity. For uncoated devices, $n_{external}$ is considered as the refractive index of air, 1. When a highly reflective (HR) coating is applied to a facet, say facet 2, reflection R_2 is presumed to be 100% or 1.

In semiconductor lasers, the active region is where laser light is generated. Thus this is the same region where light confinement would be advantageous. Greater confinement of light in the active region encourages more stimulated emission and fewer losses in the cladding regions, and thus more laser light is generated. With regards to QCL waveguides, the active region pertains to the whole superlattice structure grown within the cladding layers.

CHAPTER 3: QUANTUM CASCADE LASER GROWTH

Strain considerations are taken into account when growing the active region of QCL structure on semiconductor wafer. Each material has a lattice constant the describes the atomic spacing of the crystal lattice. When a heterostructure is grown, the mismatched lattice constants can cause strain on the overall structure. This can lead to deformities, bending, and separation of layers.

Unlike diode lasers that are mainly grown using metalorganic chemical vapor deposition (MOCVD), high-performance QCL materials are primarily grown using molecular beam epitaxy (MBE). This includes both the superlattice structure and the cladding layers of the waveguide. MBE is a very slow growth process (<20 nm per minute) where the material targets are heated such that it sublimates in vacuum onto the target. This very slow and very precise growth is required for the thinner wells of the active region. MBE growth also requires high or ultra-high vacuum (10^{-8} - 10^{-12} Torr). This high vacuum together with the slow growth rate allow for lower impurity levels in the creation of the superlattice. Also, lower growth temperature compared to that for MOCVD allows for my abrupt interfaces (lower interdiffusion).

The QCL wafer is grown as a slab waveguide. The ridge-waveguide (RWG) is formed by chemically wet etching the material away to the bottom of the superlattice. This leaves a ridge of a deigned width with an intact waveguide structure. The sidewall of the cladding layer is backfilled with silicon nitride (Si_3N_4) insulator followed by gold (Au) ohmic contact layer. Laser chips are then cleaved to size of 3 mm in length (propagation axis) and 400 μm in width.

The cleaved laser chips are initially tested using probes with point contacts. Devices with good electrical behavior (diode-like voltage characteristic) are then mounted on aluminum nitride

submounts and wire bonded. This device configuration allows for electrical current to flow evenly across the laser chip, and thus preventing localized heating due to high current density that can burn the chip from point contacts. This chip-on-carrier device is then baked, using indium-silver solder (97%In 3%Ag), onto a gold-plated copper heatsink that can be mounted and tested inside a cryostat.

CHAPTER 4: InP-BASED QCL ON GALLIUM ARSENIDE SUBSTRATE

Section 1: Goal of Monolithic Integration

The overarching goal for the silicon-based III/V optoelectronics is to combine the advantages of low cost, large substrate area epi-growth inherent to the silicon technology with the high speed and sensing capability of III/V light emitting devices. Potential defense applications include integrated platforms for man-portable or UAV-based chemical/biological sensing, environmental monitoring, out-of-band active (hyperspectral) imaging and illumination, and others. Figure 6 shows an exemplary ultra-compact infrared display with light-emitting ring-cavity pixels defined in the top III/V LED material and an integrated circuit (IC) controlling the display etched into the silicon substrate.

In this work, we demonstrated some of the main building blocks required for practical InP-based QCL-on-Si integrated platforms. The intermediary step was to develop a monolithic integration process for InP-based QCL on GaAs substrate. This was done because GaAs is exactly half the lattice mismatch between InP and Si.

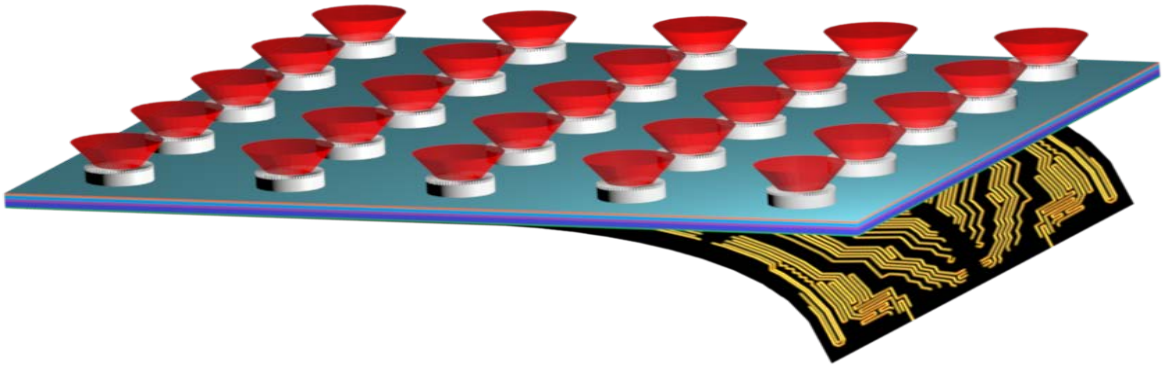

Figure 6: A concept for compact infrared display with III/V pixels defined in the top surface of the composite wafer and an IC etched into the silicon substrate.

Section 2: Design and Growth

A QCL structure with emission wavelength of 4.6 μm, a 40-stage laser core, and 8 μm-thick, all InP waveguide was grown, using proprietary metamorphic buffer (M-buffer), on a 6-inch GaAs substrate. The lattice constant of the InP waveguide is 5.86 Å, while the GaAs substrate is 5.65 Å. The active region design is shown in Figure 7. This new design is identical to the 5.6 μm QCL structure discussed in Reference [14] and shown in Figure 4, which was based on a two-material strain-balanced active region composition with a high strain both in quantum wells and barriers ($In_{0.73}Ga_{0.27}As$ and $Al_{0.78}In_{0.22}As$, respectively.) The major difference between the old 5.6 μm and the new 4.6 μm design is that the latter has an increased active region/injector coupling. This was executed to suppress carrier backscattering to the lower laser level 3 caused by a tight confinement of the active region energy states located below level 3 in the 5.6 μm design, as explained in Reference 14 (carrier extraction bottleneck). Explicitly, this modification in the design was projected to improve the laser characteristic temperature T_0, which describes the thermal behavior for laser threshold current density. The low value of T_0 was one of the main drawbacks of the 5.6 μm design. Unfortunately, this design change also led to a lower energy spacing E_{54} for the new 4.6 μm design, ranging from 72 meV to 61 meV in the bias range from 80kV/cm to 100kV/cm, respectively. This lower value of E_{54} on the new 4.6 μm design has significant consequences. Specifically, the observed lower characteristic temperature T_1 that describes dependence for laser slope efficiency can be attributed to this.

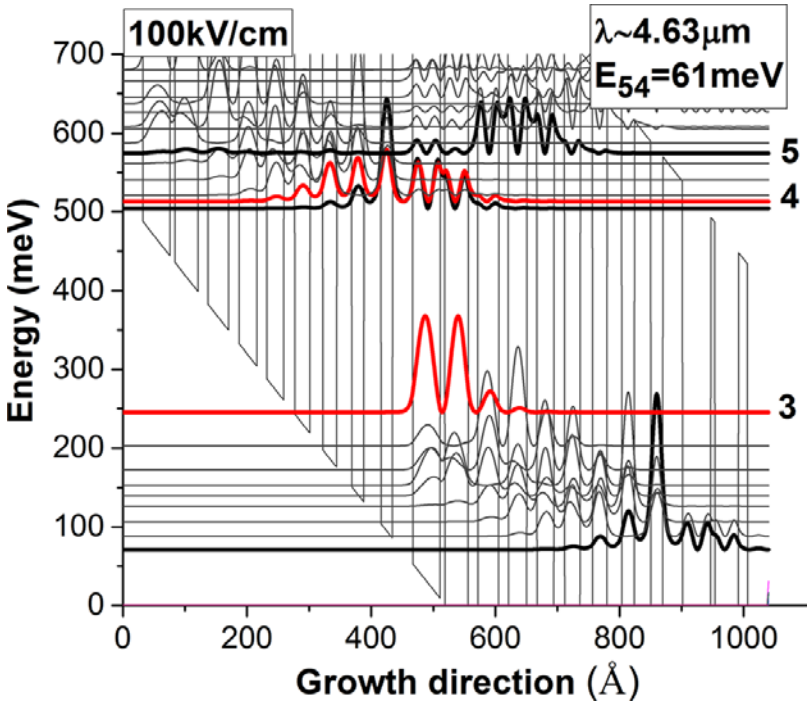

Figure 7: Active region used in this work. Band diagram at bias of 100 kV/cm for the new 4.6 μm design based on $Al_{0.78}In_{0.22}As/In_{0.73}Ga_{0.27}As$ composition. Calculated parameters at rollover: E_{54} = 61 meV and voltage defect 170 meV.

The fundamental purpose of the metamorphic buffer (M-buffer) is to accommodate the lattice mismatch between the substrate and the InP-based QCL structure. The by-product surface should have low roughness (<20 Å) for processing requirements and device reliability as elucidated in Reference 9. Semiconductor alloys like graded InAlAs and InGaAs have been used for standard production of metamorphic high electron mobility transistor circuits and have passed full reliability testing [15]. For the wafer used in this work, an InAlAs M-buffer with a linear grade to a high indium concentration was employed, proceeded by a thinner inverse grade back to the target device composition [16]. The inverse graded step was utilized to compensate for residual strain in the epitaxial layer as suggested in Reference [17]. The M-buffer's total thickness was approximately 1.1 μm. In accordance with the data reported in Reference [18], the dislocation

density is expected to be in the order of 10^9 cm^{-2} at the epi-structure/substrate interface, and reducing down to the range of 10^6 - 10^7 cm^{-2} at the top surface of the metamorphic buffer. Our future work includes full material characterization and comparison to material quality for conventional lattice-matched QCL structures. Both References [19] and [20] demonstrate that graded InGaAs buffers were considered and used for 3.0 μm to 3.5 μm QCL structure grown on GaAs substrates. In spite of that, lasing was not reported in those works.

Section 3: Surface Morphology

The surface morphology of the material growth was inspected using Nomarski optical contrast microscopy and atomic force microscopy (AFM). Figure 8 exhibits that the M-buffer grown on GaAs substrate shows a cross-hatch pattern stemming from the continual introduction of strain and ensuing relaxation through a network of misfit dislocations, a typical characteristic of this type of graded buffer scheme. The anisotropic nature of the cross-hatching is due to uneven nucleation and glide properties of the orthogonal dislocations ([1], [21], [22].) Exceptional buffer growth (see Figure 8a) is validated by the excellent root-mean-square (rms) roughness of 11 Å, where 20 Å is generally accepted as the figure-of-merit for gauging device reliability (Reference 9). Cross-hatching became more evident (see Figure 8b) for the full QCL wafer because of the additional strain build-up in the active layers, but the rms roughness remained low (11 Å).

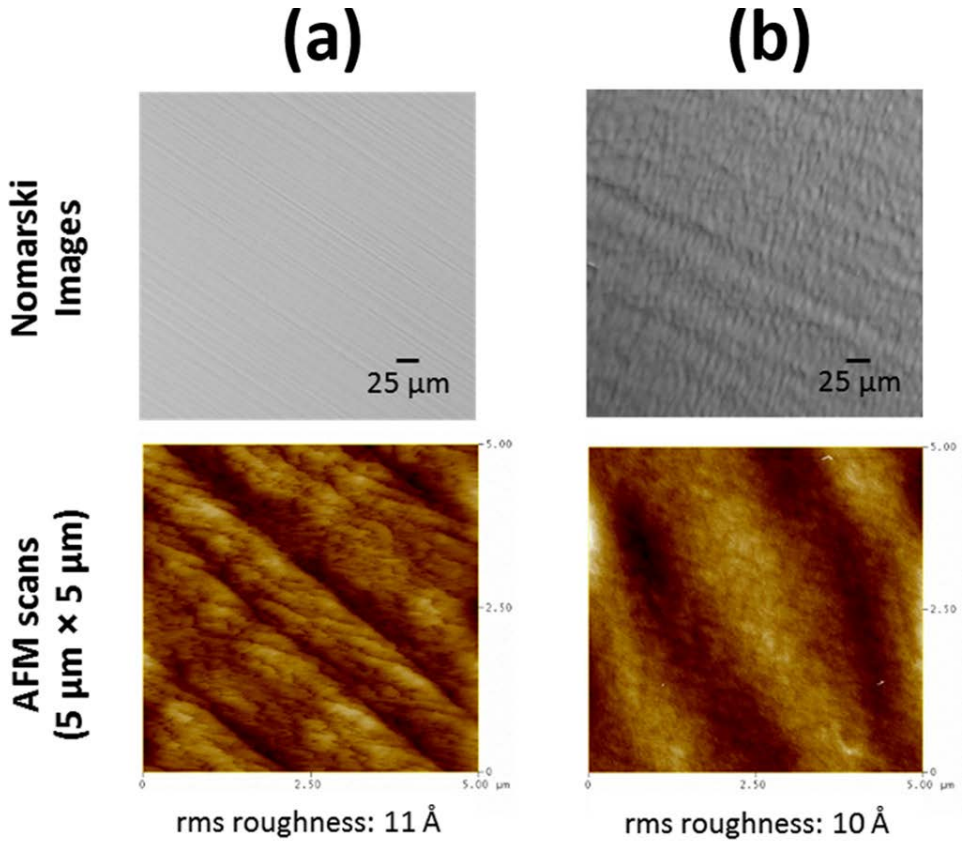

Figure 8: Nomarski optical contrast microscopy (top) and AFM images (bottom) showing cross-hatch surface morphology with low rms roughness of <20 Å for (a) graded InAlAs M-buffer and (b) full InP-QCL device structure on GaAs substrates.

Section 4: Processing

The conventional way of QCL ridge-waveguide processing utilizes symmetric injection and extraction of electrical current. The idea is to pass current through the active region in the vertical direction (from top to bottom or vice versa, depending on the device polarity and how it is mounted). Because our QCL material was grown with a special insulating metamorphic buffer between the GaAs substrate and the InP active region, we had to pattern our contact lithography photomask such that we were able to inject and extract electrical current in a highly asymmetric scheme (see Figure 9.) The current is laterally injected in the active region thru the side metal

contact, but is vertically extracted (traditional way) thru the top metal contact. This is the new technique that was introduced in our normal QCL processing. The M-buffer's insulating characteristic will allow to support an electrically independent integrated circuit to be printed on the substrate side of the wafer, if needed.

A small sample size of 2 cm^2 was cleaved from the 6-inch, 700 µm-thick QCL-on-GaAs substrate. The sample was then processed at the CREOL cleanroom and NanoScience facility. See Figure 9. First, a positive photoresist was applied to the sample wafer. After the 1st ultraviolet (UV) lithography exposure and photoresist development, the QCL ridges were formed by wet chemical etching using hydrobromic (HBr) acid. The sample was etched to the target depth of 9.5 µm. After wet etching, a 300 nm-thick insulator, silicon nitride (Si_3N_4), was deposited on the sample wafer using plasma-enhanced chemical vapor deposition (PECVD) technique. This was followed by another positive photoresist application on the patterned sample, 2nd photolithography exposure, and photoresist development. The purpose of this 2nd photolithography is to open up the InP top cladding layer while preserving the rest of the patterned sample. The InP top cladding layer was then dry etched using PECVD (the same equipment used to deposit the insulator, but with different recipe this time). Once the InP top cladding was exposed, 3rd photolithography and photoresist development ensued. The 3rd photolithography was done using negative "lift-off" photoresist, and its purpose is to form the top metal contact and the streets to isolate individual QCL chips for cleaving. The top metal contact, consisted of 20 nm of titanium (Ti) and 300 nm of gold (Au), was then deposited using electron beam (E-beam) evaporation technique. As mentioned earlier, considering the geometry of the electrical current injection/extraction scheme, the deposition of this top metallic contact would be enough for both the positive (+) and negative (-) pads to drive current through the active region. Afterwards, the sample wafer was polished

down from 700 μm to roughly 200 μm-thick to maximize the heat transfer from the QCL active region to the subsequent device mounting scheme. The bottom (substrate) side of the sample was then metallized with 20 nm Ti and 300 nm Au using E-beam evaporation (same equipment used to create the top metal contact.) The function of the bottom metallization is for soldering the individual QCL chips onto aluminum nitride (AlN) submounts in the epitaxial-up mounting configuration. Images taken using Scanning Electron Microscopy (SEM) shows the active region, etch depth, top metal contact, and side metal contact for lateral injection of current (see Figure 10). Once the material processing was done, the sample was cleaved into individual 3 mm chips. Devices were screened via pulsed testing to determine which ones were promising. Devices with 30 μm-wide ridge were mounted on AlN submount, wire bonded, then high reflection coated. The back facet was HR-coated to reduce mirror loss of the device. After coating, the chip-on-submount (CoC) device was soldered onto a gold-coated copper heat spreader. This was done for ease of handling and for testing purposes. The device on heat spreader was then placed inside a cryostat for pulsed testing (300 ns width; 10 kHz frequency) in a wide range of temperature.

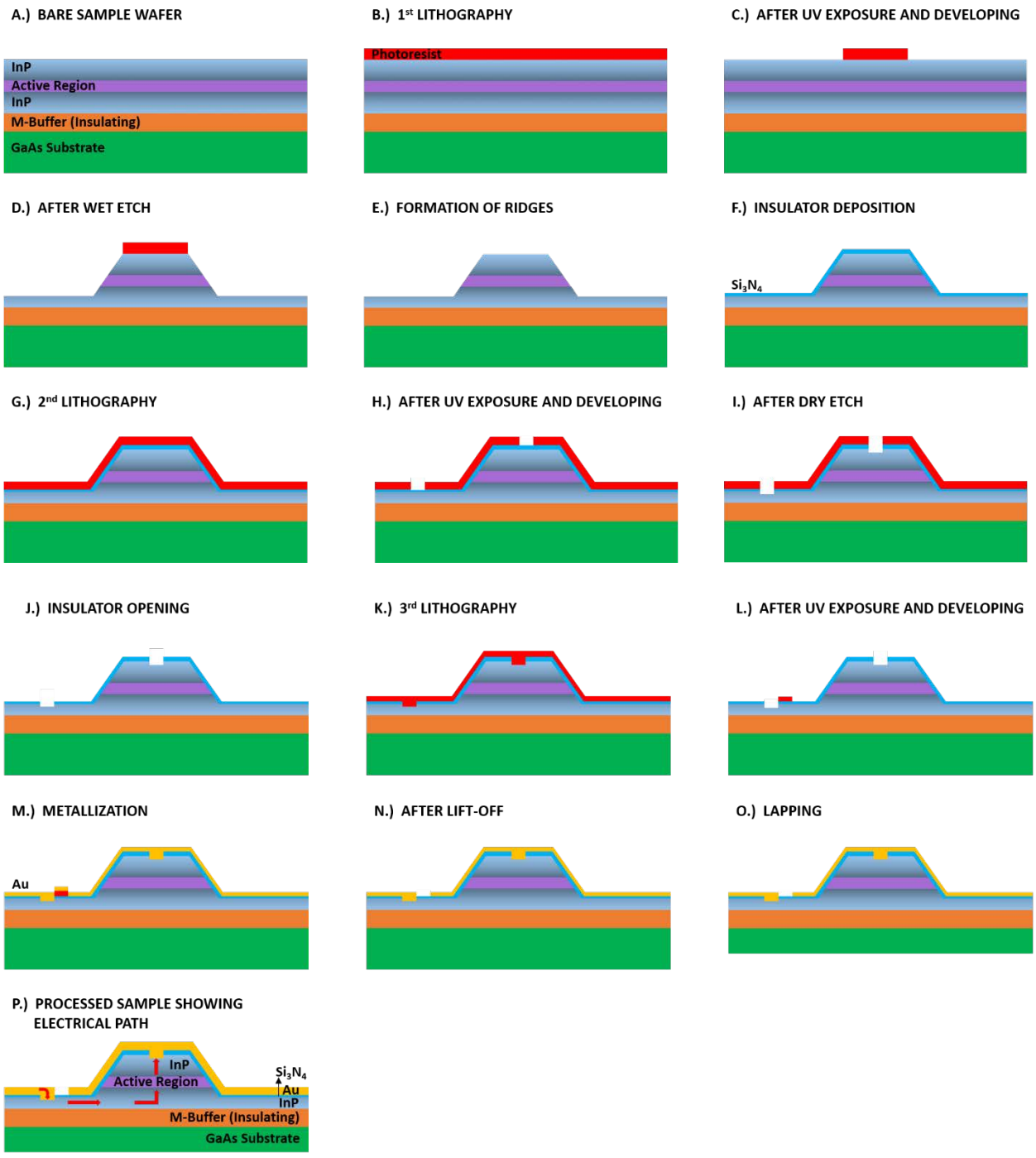

Figure 9: Step-by-step ridge-waveguide processing of InP-based QCL on GaAs substrate with insulating M-buffer.

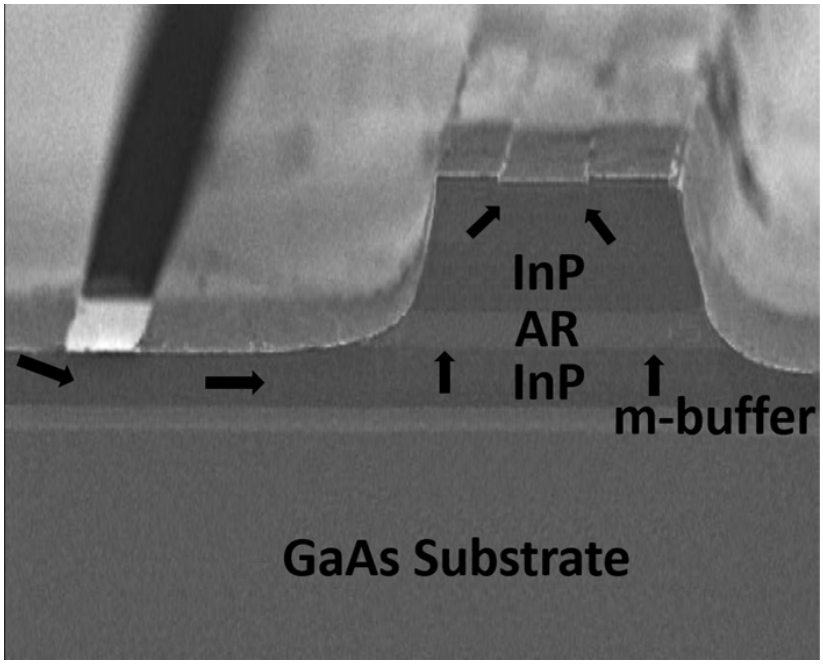

Figure 10: Scanning electron microscope image of a laser chip processed into a ridge waveguide configuration with a lateral current injection. The arrows show electrical current path (M-buffer insulating).

Section 5: Results

The device was tested from liquid nitrogen temperature (78K) and above. Figure 11 (solid lines) confer that optical power in excess of 50 mW was measured for the device up to 230 K (lasing observed all the way up to 270 K or ≈ -3 ˚C). The lasing range was further extended up to 303 K or ≈ 30 ˚C (dashed lines) by depositing a partial dielectric HR-coating (~ 56% reflectivity) to the front facet. At 293 K (room temperature, or ~ 20 ˚C), this QCL-on-GaAs substrate had threshold current density of 4.1 kA/cm^2 and maximum peak power of 15 mW. Compared to uncoated 3 mm-long device with the same active region design grown on the standard 2" InP substrate, the threshold current density is 1.3 kA/cm^2 and the pulsed efficiency is 20% at 293 K. Throughout the duration of the testing, the same device was subjected to multiple 78K to 300K thermal cycles and to ~ 200-minute preliminary reliability study (see inset for Figure 11.) There

were no signs of performance degradation that was detected. It is vital to note here that lasing was attained for the very first structure grown and tested.

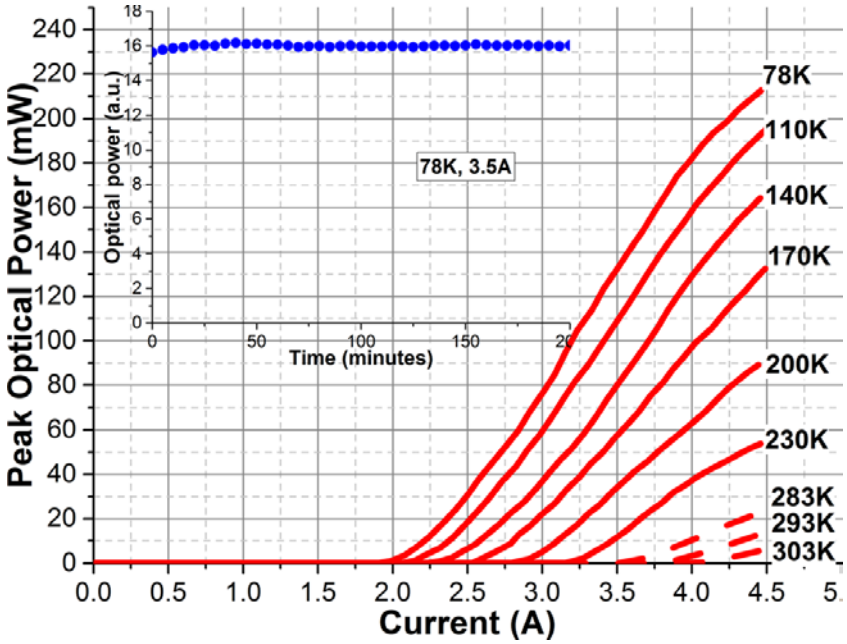

Figure 11: (solid lines) Pulsed optical power vs. current characteristics (300 ns; 10 kHz) for a 3 mm x 30 μm device with an HR-coated back facet. (dashed lines) Pulsed characteristics for the same device after and additional partial HR-coating (~56 %) was deposited on the front (output) facet of the laser. The inset shows preliminary reliability data for this device collected at 3.5 A and 78 K. No signs of performance degradation were observed.

From 78 K to 233 K, the temperature dependence for threshold current and slope efficiency can be described with characteristic temperatures $T_0 \approx 460$ K and $T_1 \approx 210$ K, respectively. The relatively high value of T_0 for this new 4.6 μm design can be attributed to the increased active region/injector coupling compared to that for the 5.6 μm design reported in Reference 14. Similarly, the lower value of T_1 can be attributed to the smaller value of E_{54}.

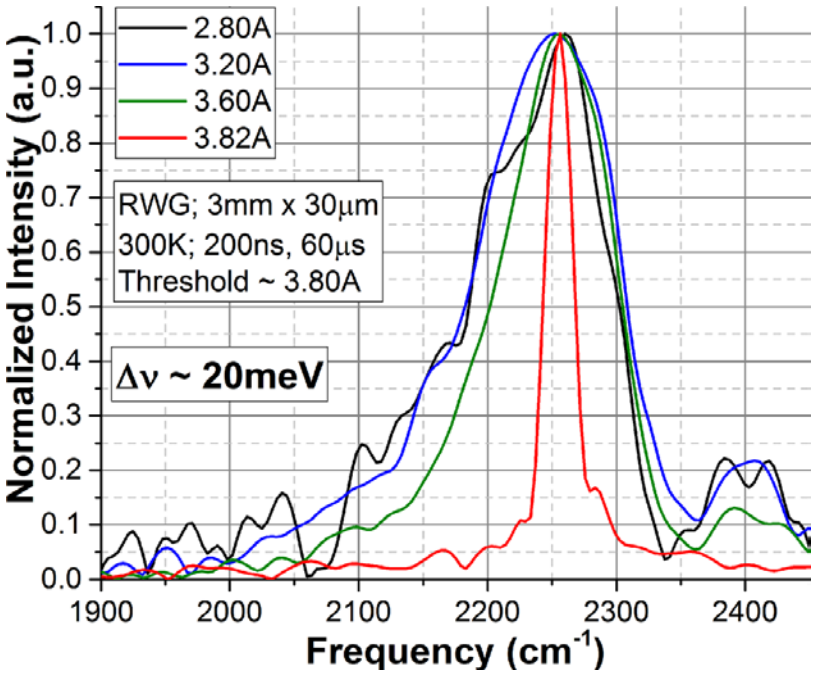

Figure 12: Laser spectrum (3.82 A) and electroluminescence spectra (2.8 A, 3.2 A, and 3.4 A) collected at 300 K. Step-scan resolution – 16 cm^{-1}. EL FWHM at low current was measured to be ~20 meV.

The spectrum for the QCL-on-GaAs was taken at set point of 3.82 A and 300 K. Wavelength was centered at 4.43 μm as can be seen on Figure 12. This is very close to the 4.65 μm central wavelength measured for the same design grown on InP substrate. The subthreshold electroluminescence (EL) of the same QCL-on-GaAs device, measured in the range from 2.80 A to 3.50 A, had a full width at half maximum (FWHM) of about 20 meV. Spectrum narrowing was noticed when the driving current exceeded 3.60 A because the operational point was moving closer to the laser threshold (~3.80 A). The fact that there is good agreement between the design (4.60 μm) and the measured (4.43 μm) emission wavelengths, together with the high value of characteristic temperature T_0 indicate that QCL growth on a lattice-mismatched substrate did not result to a significant change in the effective band diagram of the active region structure.

CHAPTER 5: InP-BASED QCL ON GERMANIUM-COATED SILICON SUBSTRATE

Section 1: Surface Morphology

An InP-based QCL structure was also grown on a 6-inch germanium coated silicon substrate utilizing M-buffers. But unlike the case for GaAs substrate, the surface morphology for the Si substrate was evaluated with two growth interruptions. The first of such interruption was after an M-buffer was grown on the Ge-coated Si substrate, and the second was after an additional 2 μm of bulk InP layer was grown on top of the M-buffer plus Ge/Si substrate. Examination of surface morphology using Nomarski optical contrast microscopy and atomic force microscopy reveal that an excellent material quality was attained in both cases (see Figure 13a and 13b). Specifically, no additional surface roughness was observed after the additional 2 μm of bulk InP layer was grown. As a matter of fact, the surface roughness improved from 17 Å to 7 Å after InP layer was grown. Based on this, we can assume that growth of additional active region layers with composition lattice-matched to InP are less likely to lead to any degradation in surface morphology since their presence would not produce any additional mechanical stress. For this reason, realization of long-wavelength infrared (8-15 μm) QCLs based on the material composition lattice-matched to InP presents a relatively low technical risk. Although extension of QCL-on-Si operation to (shorter) mid-wavelength infrared region will necessitate utilizing strained barriers and quantum wells in the active region, we believe that their realization is also likely since the overall active region design is strain-compensated.

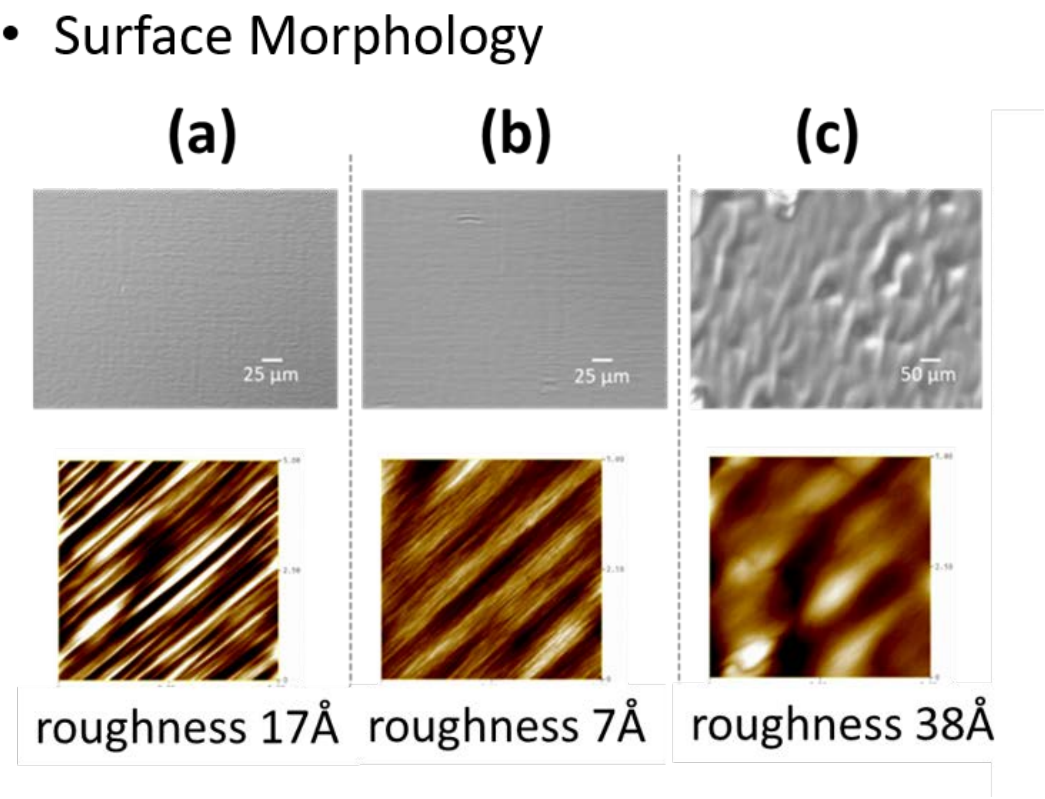

Figure 13: Nomarski (top) and AFM images (bottom) showing cross-hatch surface morphology for (a) composite M-buffer (graded InAlAs + GaAs) on Ge-coated Si substrate, (b) subsequent growth of a 2 µm InP layer, and (c) region of full InP-QCL device structure.

Section 2: Design and Growth

This work employed the same active region and waveguide QCL designs reported in [23], which allowed for direct comparison between experimental data for the two structures. The active region design had $Al_{0.78}In_{0.22}As$ barriers and $In_{0.73}Ga_{0.27}As$ quantum wells, both highly strained relative to InP bulk waveguide layers surrounding the active region (-2.04 % and 1.34 %, respectively). The employment of the high strain active region layers increases the band offset, which improves carrier confinement for MWIR QCLs and, as a consequence, increases material gain. However, while the active region was designed to have a net zero strain relative to InP, the

strain of the individual layers plus any residual net strain in the active region can make the InP-based QCL integration onto a lattice-mismatched substrate more challenging.

The QCL epitaxial wafer was produced by IQE. The 150 mm diameter Ge-on-Si substrate was created by chemical vapor deposition of a 500 nm thick Ge epilayer on Si substrate. Then, the III-V M-buffer layers and QCL device layers were grown on the Ge-Si substrate using molecular beam epitaxy (MBE). Off-axis substrates were used to help suppress anti-phase domain formation originating from polar (III-V) semiconductor on non-polar (Si) semiconductor growths by promoting bi-atomic steps on the Ge/Si surface [24].

For direct integration of InP-based QCL device structures on Si, we chose a composite metamorphic buffer consisting of GaAs (approximately 4 % lattice mismatch with Si) and graded InAlAs (compensating for the additional approximately 4 % lattice mismatch between InP and GaAs) [23]. A schematic of a composite buffer is shown in Figure 14. The QCL-on-GaAs in Reference 23 used the exact same graded InAlAs M-buffer and QCL design. Thus, the added complexity in this current work on the Ge-Si substrate is the GaAs-on-Ge nucleation and the GaAs M-buffer growth to accommodate the first half of the mismatch strain. The GaAs M-buffer unavoidably will have some residual strain, so growing the graded M-buffer plus QCL layers on it is *not* exactly like growing directly on a GaAs substrate. A full epi-layer sequence grown on the silicon substrate is shown in Figure 15.

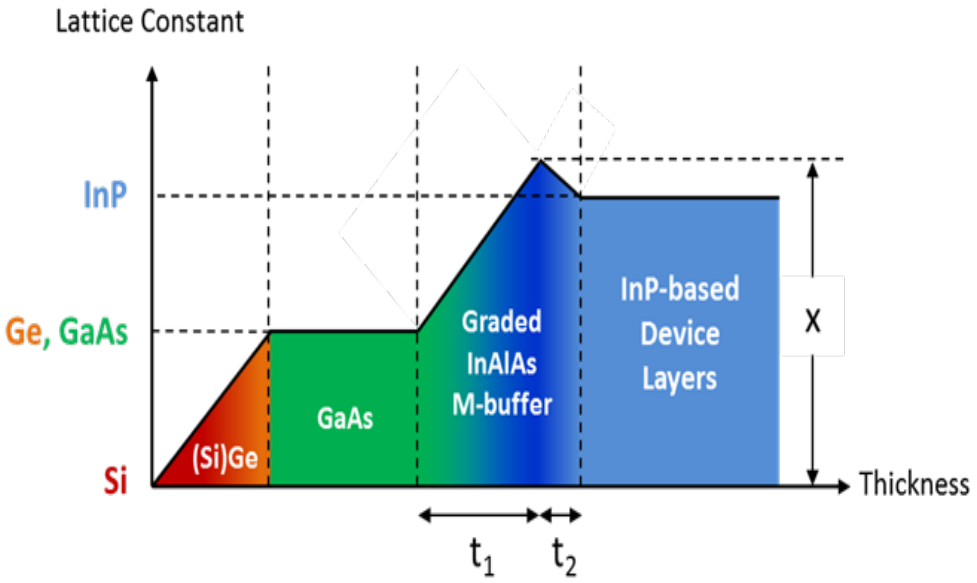

Figure 14: Schematic of composite M-buffer design that utilizes an inverse step grade for complete compensation of residual strain. InAlAs composition at the end of the M-buffer is lattice matched to InP.

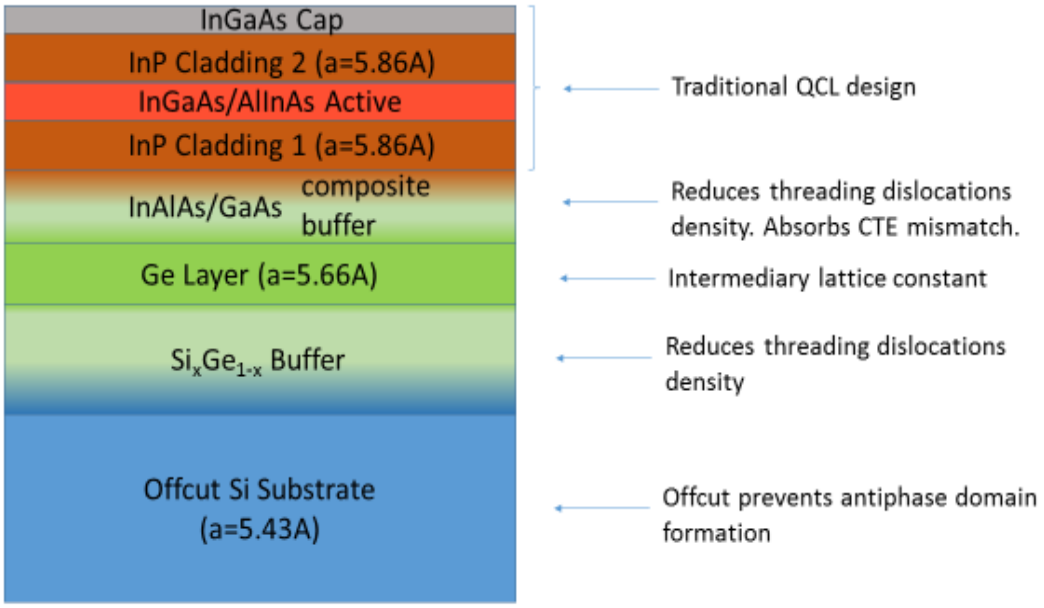

Figure 15: Schematic of the full QCL-on-Si structure.

As pointed out earlier, surface morphology of the QCL-on-Si epitaxial wafer was evaluated at various stages of the epi-stack growth using Nomarski optical contrast microscopy and atomic force microscopy (AFM), as shown in Fig. 13. A good surface morphology with a relatively low roughness was observed until QCL active region growth was carried out. The ultimate quality of the QCL-on-Si epitaxial wafer is certainly degraded compared to the QCL-on-GaAs wafer of Reference 23, which is not unexpected due to the 2× higher mismatch strain. The highly strain-compensated QCL design also affects the surface morphology. Surface areas with increased defects and/or roughness hurt device performance and yield as described below. However, there are many clear areas across the wafer where good devices were fabricated.

Section 3: Processing

Upon epi-growth, the wafer was processed into ridge-waveguide devices with lateral current injection following the processing sequence described in Reference 23. The processed wafer was cleaved into 3 mm chips. Finally, the chips were inspected under a high resolution microscope.

In contrast to QCLs-on-GaAs, most inspected chips had a poor quality of cleaved facets. The problem likely stems from a large density of threading dislocations in the epi-structure that can prevent a clean cleave propagation along the crystallographic planes. Strain release can explain debris of semiconductor material often observed on cleaved facets of the QCLs-on-Si. Through a thorough screening of the processed material, a number of chips with a good facet quality were identified for subsequent testing.

Section 4: Results

Chips with a good facet quality were mounted on submounts, wirebonded, high reflection (HR)-coated, soldered to a heat spreader, and placed in a cryostat for pulsed testing (350 ns; 2 kHz) across a broad temperature range. While lasing was observed for the very first chip tested at 78 K, overall yield of lasing devices was low (approximately 10%). In addition, in contrast to the QCL-on-GaAs material, performance for the first two chips that lased showed signs of degradation after approximately thirty minutes of operation. To minimize testing time and to reduce the additional stress for the device due to applied bias, power vs current characterization was done only up to current exceeding threshold by approximately 0.5 A.

Figure 16 shows that an HR-coated 3 mm x 40 μm device had a threshold current of 2.22 A at 78 K. Corresponding threshold current density of 1.85 kA/cm^2 is comparable to that measured for QCL-on-GaAs chips in the same configuration. At the same time, slope efficiency was approximately three times lower. The relatively low quality of the QCL-on-Si material and the relatively low yield of processed devices does not allow for a rigorous analysis of the change in laser characteristics. Lasing for the tested chip was observed up to approximately 170 K. It is important to mention here that only a small portion of the overall 6-inch wafer (2 cm^2) was processed into functional devices and a higher laser performance can likely be achieved by additional material screening.

The inset on Figure 16 shows that emission spectrum was centered essentially at the same wavelength of 4.35 μm as that for the QCL-on-GaAs material. The latter result is especially important as it demonstrates that despite the complexity of state-of-the-art QCL structures, an emission wavelength for a specific active region design can be reproduced for epi-growth on

substrates having a wide range of lattice-mismatch, provided that a proper M-buffer is used for threading dislocation density control.

The observed correlation between surface morphology and laser yield/reliability for the two structures suggests that both yield and reliability can be improved by lowering the strain of the active region layers relative to the bulk InP waveguide layers. As mentioned above, a high strain composition was used in both cases to achieve a higher material gain. However, a high MWIR QCL performance can still be achieved employing a much lower strain composition [25]. In addition, the AlInAs/InGaAs composition lattice-matched or nearly lattice-matched to InP is traditionally used in the LWIR QCL design [26]. Therefore, future work on improvement in QCL-on-Si performance should include a systematic study on finding an optimal combination of strain for the active region layers and composition of the M-buffer.

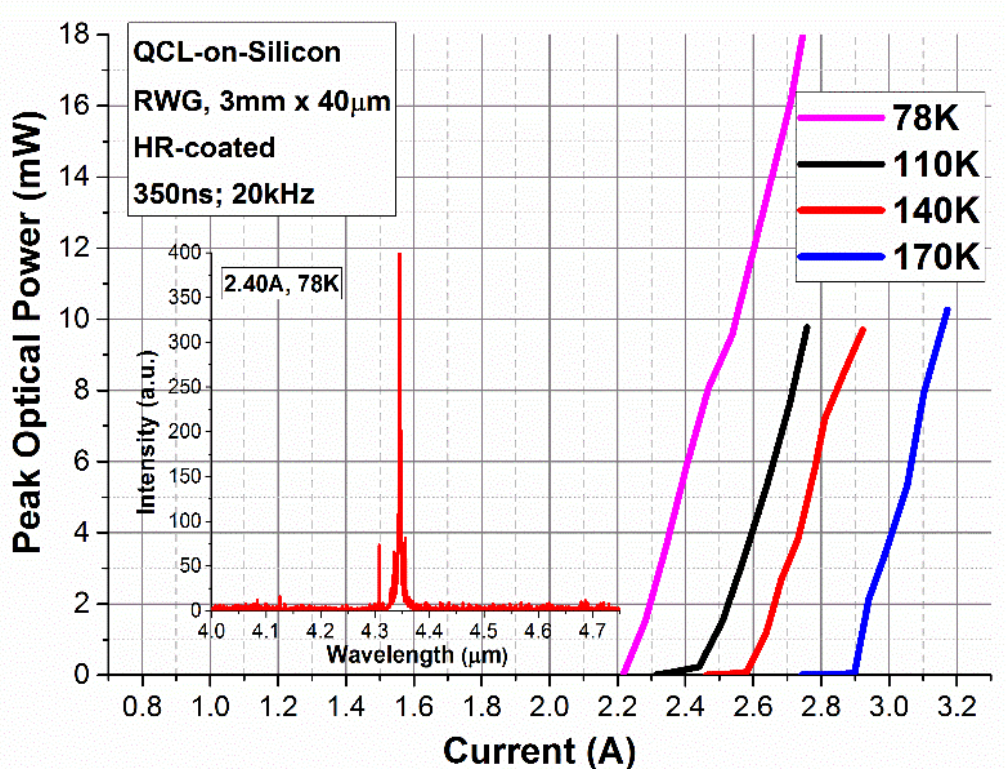

Figure 16: Pulsed optical power vs. current characteristics for a 3 mm x 40 μm device with an HR-coated back facet measured in temperature range of 78 K to 170 K. Inset: spectrum measured at 2.40 A and 78 K.

CHAPTER 6: CONCLUSIONS

In conclusion, the first room temperature operation for InP-based QCLs monolithically grown on lattice-mismatched substrate with an M-buffer has been demonstrated. For QCL grown on GaAs substrate, lasing from cryogenic temperature (78 K) up to 230 K was observed for a 3mm x 30 μm device with HR-coated back facet. Lasing was extended above room temperature (30 °C) by applying additional partial HR coating to the front facet. No power degradation was detected after 200 minutes of short-term burn-in. The measured characteristic temperatures are in the proximity of typical values reported for traditional QCLs grown on InP substrates. Analyses of surface morphology using AFM and optical microscopy suggest that a higher material quality, and thus higher laser performance, is achievable by lowering the strain of the active region layers.

Lasing from 78 K up to 170 K was also demonstrated for an InP-based QCL structure grown on a Ge-coated silicon wafer via a III-V M-buffer. Devices with 3 mm x 40 μm dimensions and HR-coated back facets were tested. Measured emission wavelength was close to its design value. The presented data suggest that the observed low yield and reliability can be both improved by reducing strain of the active region layer relative to the bulk InP waveguide layers surrounding the active region.

This work has demonstrated some of the main building blocks necessary for practical QCL-on-Si integrated platforms. Future work will include in-depth study of the misfit dislocations for QCL on lattice-mismatched substrate. We will also try to grow longer wavelength QCL on Ge-coated Si substrate. By utilizing strain free active region design for longer wavelengths, we believe that we can improve the device performance and that we will achieve higher yield and reliability. When successfully implemented, this will set a new research and development direction for Si-

based photonics and will pave the way for the development of ultra-compact infrared displays, sensors, beacons, illuminators, and other infrared platforms with game changing characteristics for critical Department of Defense applications.

LIST OF REFERENCES

1. Faist, J., et al., *Quantum Cascade Laser.* Science, 1994. **264**(5158): p. 553-556.

2. Nasim, H. and Y. Jamil, *Diode lasers: From laboratory to industry.* Optics & Laser Technology, 2014. **56**(Supplement C): p. 211-222.

3. Kazarinov, R.F. and R.A. Suris, *Electric and electromagnetic properties of semiconductors with a superlattice*. Vol. 6. 1972. 120-131.

4. Borri, S., *Comb-referenced spectroscopy with quantum cascade lasers*. 2009. p. 1.

5. Theisen, L.A. and K.L. Linker, *Quantum Cascade Lasers (QCLs) for standoff explosives detection : LDRD 138733 final report*. 2009, ; Sandia National Laboratories. p. Medium: ED; Size: 19 p.

6. *Daylight Defense[TM] Successfully Completes Environmental Testing of Fourth Generation Quantum Cascade Laser (QCL) System for Infrared Countermeasures*. 2011, Business Wire, Inc.

7. Faist, J., et al., *Coherent frequency combs produced by self frequency modulation in quantum cascade lasers*.

8. Pilling, M.J., A. Henderson, and P.p.g.m.a.u. Gardner, *Quantum Cascade Laser Spectral Histopathology: Breast Cancer Diagnostics Using High Throughput Chemical Imaging.* Analytical Chemistry, 2017. **89**(14): p. 7348-7355.

9. Heck, M.J.R., et al., *Hybrid Silicon Photonic Integrated Circuit Technology.* IEEE Journal of Selected Topics in Quantum Electronics, 2013. **19**(4): p. 6100117-6100117.

10. Hofstetter, D., M. Beck, and J. Faist, *Quantum-cascade-laser structures as photodetectors.* Applied Physics Letters, 2002. **81**(15): p. 2683-2685.

11. Hugi, A., et al., *Mid-infrared frequency comb based on a quantum cascade laser.* Nature, 2012. **492**: p. 229.

12. Mujagić, E., et al., *Low divergence single-mode surface emitting quantum cascade ring lasers.* Applied Physics Letters, 2008. **93**(16): p. 161101.

13. Yamaguchi, M. and C. Amano, *Efficiency calculations of thin-film GaAs solar cells on Si substrates.* Journal of Applied Physics, 1985. **58**(9): p. 3601-3606.

14. Lyakh, A., et al., *5.6 μm quantum cascade lasers based on a two-material active region composition with a room temperature wall-plug efficiency exceeding 28%.* Applied Physics Letters, 2016. **109**(12): p. 121109.

15. E. Leoni, R., et al., *GaAs-Based Metamorphic Technology*, in *2002 International Conference on Compound Semiconductor Manufacturing Technology Digest of Papers*. 2002, GaAs MANTECH: St. Louis. p. 272-275.

16. Lubyshev, D., et al., *Comparison of As- and P-based metamorphic buffers for high performance InP heterojunction bipolar transistor and high electron mobility transistor applications.* Journal of Vacuum Science & Technology B: Microelectronics and Nanometer Structures Processing, Measurement, and Phenomena, 2004. **22**(3): p. 1565-1569.

17. Cordier, Y. and D. Ferré, *InAlAs buffer layers grown lattice mismatched on GaAs with inverse steps.* Journal of Crystal Growth, 1999. **201-202**: p. 263-266.

18. Lubyshev, D., et al., *Strain relaxation and dislocation filtering in metamorphic high electron mobility transistor structures grown on GaAs substrates.* Journal of Vacuum Science & Technology B: Microelectronics and Nanometer Structures Processing, Measurement, and Phenomena, 2001. **19**(4): p. 1510-1514.

19. Mawst, L.J., et al., *InGaAs/AlInAs strain-compensated Superlattices grown on metamorphic buffer layers for low-strain, 3.6μm-emitting quantum-cascade-laser active regions.* Journal of Crystal Growth, 2013. **370**: p. 230-235.

20. Rajeev, A., et al., *Regrowth of quantum cascade laser active regions on metamorphic buffer layers.* Journal of Crystal Growth, 2016. **452**: p. 268-271.

21. E. Lefebvre, M.Z., Y. Cordier, and F. Mollot. in *15th Indium Phosphide and Related Materials Conference*. May 2003. Santa Barbara, CA.

22. Chauveau, J.-M., et al., *Interplay between relaxation, surface morphology and composition modulation in InAlAs graded buffer layers.* Journal of Crystal Growth, 2003. **251**(1): p. 112-117.

23. Go, R., et al., *Room temperature operation of quantum cascade lasers monolithically integrated onto a lattice-mismatched substrate.* Applied Physics Letters, 2018. **112**(3): p. 031103.

24. Ting, S.M. and E.A. Fitzgerald, *Metal-organic chemical vapor deposition of single domain GaAs on Ge/GexSi1−x/Si and Ge substrates.* Journal of Applied Physics, 2000. **87**(5): p. 2618-2628.

25. Lyakh, A., et al., *1.6W high wall plug efficiency, continuous-wave room temperature quantum cascade laser emitting at 4.6μm.* Applied Physics Letters, 2008. **92**(11): p. 111110.

26. Xie, F., et al., *Impact of Wavelength Detuning on the Performance of Mid-IR Distributed Feedback Quantum Cascade Lasers.* IEEE Journal of Selected Topics in Quantum Electronics, 2013. **19**(4): p. 1200508-1200508.